Study of the angular distributions of the reactions

$$\bar{p}p \to \chi_{c1}, \chi_{c2} \to J/\psi\,\gamma \to e^+e^-\gamma$$

M. Ambrogiani,[2] S. Bagnasco,[6] W. Baldini,[2] D. Bettoni,[2] G. Borreani,[6] A. Buzzo,[3]

R. Calabrese,[2] R. Cester,[6] P. Dalpiaz,[2] X. Fan,[5] G. Garzoglio,[1] K. Gollwitzer,[1]

A. Hahn,[1] S. Jin,[5] J. Kasper,[5] G. Lasio,[4] M. LoVetere,[3] E. Luppi,[2] P. Maas,[5]

M. Macrì,[3] M. Mandelkern,[4] F. Marchetto,[6] M. Marinelli,[3] E. Menichetti,[6] R. Mussa,[2,6]

M. Obertino,[6] M. Pallavicini,[3] N. Pastrone,[6] C. Patrignani,[3] T. Pedlar,[5] S. Pordes,[1]

E. Robutti,[3] J. Rosen,[5] P. Rumerio,[6] A. Santroni,[3] M. Savrié,[2] J. Schultz,[4] K. K. Seth,[5]

G. Stancari,[2] M. Stancari,[4] J. Streets,[1] A. Tomaradze,[5] S. Werkema,[1] and G. Zioulas[4]

(Fermilab E835 Collaboration)

[1]*Fermi National Accelerator Laboratory, Batavia, Illinois 60510*

[2]*Istituto Nazionale di Fisica Nucleare and University of Ferrara, 44100 Ferrara, Italy*

[3]*Istituto Nazionale di Fisica Nucleare and University of Genova, 16146 Genova, Italy*

[4]*University of California at Irvine, California 92697*

[5]*Northwestern University, Evanston, Illinois 60208*

[6]*Istituto Nazionale di Fisica Nucleare and University of Torino, 10125 Torino, Italy*

(Dated: October 29, 2001)

Abstract

We report on a study of the angular distributions in the radiative decay of the χ_{c1} and χ_{c2} states formed in $\bar{p}p$ annihilations. These distributions depend on the dynamics of the formation process and the multipole structure of the radiative decay. Using 2090 χ_{c1} and 5908 χ_{c2} events, we have measured the fractional magnetic quadrupole amplitude to be $a_2(\chi_{c1}) \simeq$ M2/E1$= 0.002 \pm 0.032$, and $a_2(\chi_{c2}) = -0.093^{+0.039}_{-0.041}$. We have also measured the square of the helicity 0 fractional amplitude in the χ_{c2} formation process to be $B_0^2 = 0.13 \pm 0.08$.

I. INTRODUCTION

Experiment E835 at Fermilab [1] is a continuation of the study of charmonium states started by Experiment E760 [2], with a substantial upgrade to facilitate higher luminosity operation. During the 1996-97 run, E835 collected data corresponding to an integrated luminosity of 5.8 pb^{-1} in the χ_{c1} energy region, and 11.2 pb^{-1} at the χ_{c2}. In this paper we present the results of the analysis of the angular distribution for the processes:

$$\bar{p}p \to \chi_{c1}, \chi_{c2} \to J/\psi \; \gamma \to e^+ e^- \gamma \tag{1}$$

The angular distribution for this production/decay sequence is sensitive to the features of the $\bar{p}p$ annihilation process, the properties of the $c\bar{c}$ bound state and the nature of its radiative decay. The study of exclusive charmonium production and decay channels has long been recognised as a good testing ground for bound state models. The coupling between the set of charmonium χ states and $\bar{p}p$ is described by four independent helicity amplitudes. χ_{c0} is formed only through the helicity 0 channel, χ_{c1} can be formed only through the helicity 1, and χ_{c2} can couple through both; the relative strength of these last two amplitudes can be measured only from the study of the angular distribution.

The χ_c radiative decay is dominated by the dipole term E1. The higher multipoles, M2 and E3, arise in the relativistic treatment of the interaction between the electromagnetic field and the quarkonium system (see, for example,[3]). These terms give contributions at a few percent level to the radiative width:

$$\Gamma(\chi_c \to J/\psi\gamma) = |E1|^2 + |M2|^2 + |E3|^2 = |E1|^2(1 + \mathcal{O}(E_\gamma^2/m_c^2)) = |E1|^2(1 + \mathcal{O}(10^{-2}))$$

The study of the radiative decay angular distributions of the χ_{c1} and χ_{c2} states allows the measurement of the deviation from pure E1 transition[4], through the E1-M2 and E1-E3 interference terms.

The fractional electric octupole amplitude, labeled as $a_3 \simeq$ E3/E1, can contribute only to the χ_{c2} decay, and is predicted to vanish in the single quark radiation model [5], if the J/ψ is a pure S-wave state. Even if there is an admixture of D-wave, a_3 is expected to be negligibly small [6, 7].

In the description of the χ_c radiative decay, the dominant terms of both E1 and M2 amplitudes contain the same overlap integral of the initial and final states radial wavefunctions; relativistic effects on the wavefunctions are expected to cancel out in the fractional

amplitudes, labeled as $a_2 \simeq$ M2/E1 . A relativistic calculation [6] at order $(v_c/c)^2$ yields the relations [1]:

$$a_2(\chi_{c1}) = -\frac{E_\gamma}{4m_c}(1 + \kappa_c) \qquad\qquad a_2(\chi_{c2}) = -\frac{3}{\sqrt{5}}\frac{E_\gamma}{4m_c}(1 + \kappa_c)$$

The parameter κ_c measures the deviation of the magnetic moment from that of a free Dirac charm quark (i.e. $\mu_c = \frac{2}{3}\frac{e}{2m_c}$, with $\hbar$=c=1). Using E_γ=389.6 MeV and 429.4 MeV for the χ_{c1} and χ_{c2} decays respectively, and assuming m_c=1.5 GeV/c^2, we have $a_2(\chi_{c1}) = -0.065(1+\kappa_c)$ and $a_2(\chi_{c2}) = -0.096(1 + \kappa_c)$.

The ratio between the fractional M2 amplitudes measured for the two decays can provide a check of the basic assumptions of the derivation; it gives:

$$\left.\frac{a_2(\chi_{c1})}{a_2(\chi_{c2})}\right|_{th} = \frac{\sqrt{5}}{3}\frac{E_\gamma(\chi_{c1})}{E_\gamma(\chi_{c2})} = 0.676 \tag{2}$$

In fact, present data are not in agreement with this prediction but the comparison requires taking measurements from two quite different experiments, E760 ($a_2(\chi_{c2})$, ref.[8]) and Crystal Ball ($a_2(\chi_{c1})$, ref.[9]), and may be considered sensitive to different systematics. E835 has now measured both these quantities with adequate precision in one experiment.

II.   ANGULAR DISTRIBUTION IN THE HELICITY FORMALISM

The angular distribution of reaction (1) is a function of three angles θ, θ' and ϕ', which are defined as follows (see Fig. 1):

θ: the polar angle of the J/ψ with respect to the antiproton, in the $\bar{p}p$ center-of-mass system;

θ': the polar angle of the positron in the J/ψ rest frame with respect to the J/ψ direction in the χ center of mass system;

ϕ': the azimuthal angle between the J/ψ decay plane and the χ_c decay plane, defined by the expression [2]:

$$\cos\phi' = \frac{(\vec{\mathbf{p}}_{J/\psi} \times \vec{\mathbf{p}}_{\bar{p}})}{\parallel \vec{\mathbf{p}}_{J/\psi} \times \vec{\mathbf{p}}_{\bar{p}} \parallel} \cdot \frac{(\vec{\mathbf{p}}_{J/\psi} \times \vec{\mathbf{p}}_{e^+})}{\parallel \vec{\mathbf{p}}_{J/\psi} \times \vec{\mathbf{p}}_{e^+} \parallel}$$

---

[1] We have corrected a misprint in Eq.41 of ref. [6].

[2] Since the positron cannot be distinguished from the electron in our detector, θ' is allowed to range from 0 to $\pi/2$; since all the distributions are symmetric in ϕ', ϕ' can range from 0 to π

Using the helicity formalism and the above definitions, the angular distribution for reaction 1 can be written as [10, 11]

$$W(\theta, \theta', \phi') = \sum_i K_i(B_{|\lambda(\bar{p})-\lambda(p)|}, A_{|\lambda(J/\psi)-\lambda(\gamma)|})T_i(\theta, \theta', \phi') \qquad (3)$$

where the coefficients K_i depend upon the helicity amplitudes and the T_i's are functions of the observed angles θ, θ', ϕ'. The index $\lambda(\bar{p}) - \lambda(p)$ is equal to the projection of the χ_c spin on the $\bar{p}$ direction, and $\lambda(J/\psi) - \lambda(\gamma)$ is the projection of the χ_c spin on the J/ψ direction.

The detailed expression for the angular distribution is given in the Appendix. The helicity amplitudes $B_{|\lambda(\bar{p})-\lambda(p)|}$ and $A_{|\lambda(J/\psi)-\lambda(\gamma)|}$ parametrize the dynamics of the formation and of the decay processes, respectively. In the formation process of the χ_{c1}, charge conjugation (C) invariance requires $B_0 \equiv 0$, and $B_1 = -B_{-1}$. For the χ_{c2}, C invariance implies that $B_1 = B_{-1}$; B_0 can differ from zero.

The helicity amplitudes $A_0, .., A_J$ can be expressed as linear combinations of the multipole transition amplitudes $a_1, ..., a_{J+1}$ (see Appendix, eqs.7 and 8), which are related to the total angular momentum carried away by the photon. Since χ_{cJ} and J/ψ have opposite parities, the amplitudes a_1, a_2 and a_3 correspond to electric dipole (E1), magnetic quadrupole (M2) and electric octupole (E3) transitions, respectively.

The normalization conditions

$$\sum_{i=-1}^{1} B_i^2 = 1 \quad ; \quad \sum_{k=0}^{J} A_k^2 \equiv \sum_{m=1}^{J+1} a_m^2 = 1$$

imposed on the helicity amplitudes further reduce the number of independent parameters. Conventionally $a_2(\chi_{c1})$, $a_2(\chi_{c2})$, $B_0^2(\chi_{c2})$ and $a_3(\chi_{c2})$ are chosen as the independent parameters to be determined, and $a_1(\chi_{c1})$ and $a_1(\chi_{c2})$ are taken to be positive.

III.   EXPERIMENT LAYOUT

A.   The E835 target and antiproton beam

The experiment is located in the AP-50 straight section of the Fermilab Antiproton Source complex. Stochastically cooled antiprotons stored in the Accumulator collide with an internal molecular hydrogen jet target [12]. The interaction region measures $5mm \times 5mm \times 6mm$. An instantaneous luminosity L $\sim 2 \times 10^{31} cm^{-2} s^{-1}$ was achieved during most of the data taking.

B.   The detector

The detector (see Fig. 2) is a non-magnetic, large acceptance spectrometer with cylindrical symmetry about the beam axis. It is optimized for the detection of electromagnetic final states and allows the rejection of the very high hadronic background. The detector has been substantially upgraded with respect to the one used for the E760 experiment, by adding pulse shaping and TDC readout on all the counters, to allow for the higher interaction rate. The central detector is built in concentric cylindrical layers. Two sets of scintillator hodoscopes H1 and H2 (with 8-fold and 32-fold azimuthal segmentation, respectively) are used for charged event triggering. Four layers of straw tubes [13] provide azimuthal information for charged tracks and a pair of layers of scintillating fibers [14] provide information on the polar angle.

A threshold Čerenkov counter [15], with 8-fold azimuthal and 2-fold polar segmentation, is used for electron identification and covers the full azimuth and the polar range $15° \leq \theta_{lab} \leq 65°$. The septum between the two polar regions was modified for E835 to avoid any loss of efficiency in the septum region.

The outermost component of the central detector is a lead glass electromagnetic Central Calorimeter (CCAL) [16], with full azimuthal acceptance and uniform polar acceptance from $10°$ to $70°$. It consists of 1280 counters pointing to the interaction region, which are arranged into 20 polar "rings" and 64 azimuthal "wedges". The CCAL measures the energy of electrons and photons, with a resolution $\sigma_E/E \approx 0.014 + 0.06/\sqrt{E(GeV)}$, and, coupled with the known position and size of the interaction region, provides a measurement of the polar and azimuthal angles, with resolutions $\sigma_\theta = 6 \, \mathrm{m}rad$ and $\sigma_\phi = 11 \, \mathrm{m}rad$. The forward region is instrumented with an 8-element scintillator hodoscope (used as a charged particle veto at trigger level), and a Forward Calorimeter (FCAL), which was not used in this analysis.

The absolute luminosity is measured by an array of three solid state detectors [17], which count recoil protons scattered elastically at $\theta_{lab} \simeq 86.5°$.

6

IV.   TRIGGER AND EVENT SELECTION

A.   Trigger requirements

The first level of the trigger logic is designed to select high mass objects decaying to e^+e^- with high efficiency [18]. The essential elements entering the trigger are: logic signals from the 16 Čerenkov cells, the scintillator hodoscopes (H1 and H2), and a matrix of 5 (θ_{lab}) x 8 (ϕ_{lab}) analog sums from the Central Calorimeter. The analog sums from the central calorimeter coarsely define the positions and energies of electromagnetic showers (clusters).

The primary trigger requires that a Čerenkov signal be associated with each of two charged tracks originating from the interaction region, as defined by an appropriate coincidence between elements of the H1 and H2 hodoscopes. In order to select two body decays of massive objects, it requires two clusters in the CCAL, separated by more than 90° in azimuth and with energies above thresholds which depend on the polar angle. The number of accompanying charged particles is limited by the requirement of ≤ 5 hits in the H2 hodoscope.

Two additional triggers are implemented to monitor and study Čerenkov and CCAL efficiencies. The first auxiliary trigger (AT1) requires that only one of the two charged tracks be tagged as an electron by the Čerenkov, while in the second auxiliary trigger (AT2) the requirement on the CCAL is removed. In both cases, to keep the rate to a reasonable level, only events with charged particle multiplicity of 2 (defined by the number of H2 hits) are accepted, with the coplanarity constraint requiring the two charged tracks back to back in azimuth within 22.5^o. An additional veto on charged tracks in the forward region is imposed on trigger AT2.

The primary trigger selects 96% of the events, while 4% are recovered by the auxiliary trigger AT1. The loss of events related to the tighter coplanarity requirements in AT1 is negligible. Event loss due to CCAL inefficiency is also negligible.

The efficiency of the coincidence H1⊗H2 was studied [18] with a set of dedicated runs and monitored throughout the data taking with samples of minimum bias events. The dedicated runs were also used to evaluate possible biases due to θ-dependent efficiencies of the hodoscopes. No significant effect was observed.

B. Software event selection

The selection of $\chi \to J/\psi\gamma \to e^+e^-\gamma$ events is based on the number of clusters and on a 5C kinematic fit. We require that the three final state particles be detected in the CCAL. One extra cluster is allowed, if its energy is smaller than 200 MeV, to avoid rejection of the fraction of events (about 10%) where one bremsstrahlung photon is emitted by the electron or positron.

Fiducial cuts on the electrons ($15° < \theta_{lab} < 60°$) and on the photon ($12° < \theta_{lab} < 68°$) are imposed to avoid edge effects. An additional cut ($|\cos\theta'| < 0.95$) is used to discard events where the CCAL clusters for the electron and the photon overlap.

A 5C fit is performed using the measured energies and directions of the two electrons and the photon. The low background level allows us to set a low threshold on the kinematic fit probability (CL$> 10^{-3}$) thus reducing any systematic effects from imperfect knowledge of the calorimeter resolution.

The numbers of events surviving these cuts are 2090 at the χ_{c1}, and 5908 at the χ_{c2}; we estimate that 1.1 to 1.8 percent of the event samples are background (mostly due to non resonant $3\pi^o$ events), as measured from the event rate outside the resonance region.

V. ANALYSIS OF THE ANGULAR DISTRIBUTION

The maximum likelihood method is used to estimate the values of the angular distribution parameters. As mentioned at the end of section II, we fit for helicity amplitudes in the formation process and multipole amplitudes in the decay. The unbinned likelihood function is defined as

$$\mathcal{L}(\alpha) = \prod_{j=1}^{N_{events}} P_j(\alpha; \Omega_j)$$

where Ω_j spans the variable space $\{\cos\theta_j, \cos\theta'_j, \phi'_j\}$, and α spans the fit parameter space: $\{a_2\}(\chi_{c1})$ and $\{B_0^2, a_2, a_3\}(\chi_{c2})$. The probability density P_j of observing an event at Ω_j is a function of the parameters, and is given by

$$P_j(\alpha; \Omega_j) = \frac{W(\alpha; \Omega_j) \cdot acc(\Omega_j)}{\int W(\alpha; \Omega) \cdot acc(\Omega) \, d\Omega} \tag{4}$$

Here W is the theoretical distribution function (Eq. 3), $acc(\Omega)$ is the geometric acceptance function, and the integral in the denominator is performed over the entire variables space.

The difficulty of performing a 3-dimensional integral for each point in the α space in order to maximize the likelihood function can be overcome if we recall that W can be factorized into angle-dependent and amplitude-dependent terms (see Eq. 3). Using this property, the denominator of Eq. 4 can be written as

$$\int W(\alpha; \Omega) \cdot acc(\Omega) \, d\Omega = \sum_i K_i(\alpha) \cdot F_i$$

where the terms $F_i = \int T_i(\Omega) \cdot acc(\Omega) \, d\Omega$ are independent of the dynamics, and can be calculated for any acceptance configuration using a Monte Carlo integration method. The estimates of the angular distribution parameters α are found by maximizing the logarithm of $\mathcal{L}(\alpha)$.

The goodness of fit is estimated using the χ^2 method. The data are binned into 120 bins, 6 in $\cos\theta$ (-0.81 to 0.81, δ_{bin}=0.27), 5 in $\cos\theta'$ (0 to 0.95, δ_{bin}=0.19), and 4 in ϕ' (0 to π, $\delta_{bin}=\pi/4$), and the χ^2 is calculated using [19]

$$\chi^2 = \sum_{i=1}^{120} (2(n_i^{pred} - n_i^{obs}) + 2n_i^{obs} ln(n_i^{obs}/n_i^{pred}))$$

where n_i^{obs} is the observed and n_i^{pred} is the expected number of events in the i-th bin, normalized to N_{events}.

VI.   RESULTS

The results of the likelihood fits are summarized in tables I and II. The statistical errors are determined from the contour on which the likelihood function has decreased by a factor $e^{-\frac{1}{2}}$. The χ^2 for all fits is satisfactory and the best fit values derived by minimizing the χ^2 are consistent with those obtained maximizing the likelihood. The number of degrees of freedom varies with the number of free parameters, and with the number of bins within the acceptance.

A.   Results for the χ_{c1}

The full χ_{c1} angular distribution is given in the Appendix. The E1-M2 interference term is given by:

$$\Delta W = a_1 a_2 (\cos^2\theta - \cos^2\theta')$$

For a pure dipole transition, $a_1=1$, the angular distribution is given by:

$$W(\cos\theta, \cos\theta', \phi') = \frac{1}{2}(1 - \cos^2\theta\cos^2\theta' - \sin\theta\cos\theta\sin\theta'\cos\theta'\cos\phi')$$

The effect of $a_2 \neq 0$ would be to introduce an asymmetry between θ and θ' in the angular distribution. The observed numbers of events are compared in Fig.3 with the best fit expectations. Each table shows the ϕ', $\cos\theta'$ event numbers for one $\cos\theta$ bin; the binning is defined in section V.

In Fig.4, we show the projections of the χ_{c1} angular distribution, on the three observables $\cos\theta$, $\cos\theta'$ and ϕ'. The shaded histograms give the observed number of events, uncorrected for acceptance. The dots indicate the event numbers after acceptance corrections, and the line histograms show best fit predictions.

As an illustration, if $a_2 = 0$, the projections of the angular distributions reduce to:

$$\bar{W}(\cos\theta) \sim 1 - \frac{1}{3}\cos^2\theta \quad ; \quad \bar{W}(\cos\theta') \sim 1 - \frac{1}{3}\cos^2\theta'$$

After the acceptance corrections, the ϕ' projection is expected to be flat for any value of a_2.

The best fit value of a_2 for the χ_{c1} resonance is $a_2 = 0.002 \pm 0.032$, as reported in Table I. The χ^2 is 87.3, with N_{dof}=96.

Minimum χ^2 and maximum likelihood methods give fully compatible results $(a_2(\text{likelihood})\text{-}a_2(\chi^2)\text{=-0.002})$. Fig.5 shows that -ln($\mathcal{L}$) is smooth and well behaved over the whole parameter space; local minima of -ln($\mathcal{L}$) are also visible at $a_2 = \pm 1$ (i.e. $a_1 = 0$), with $\chi^2 \approx 140$.

By adding events from the samples of data taken above and below the χ_{c1} CM energy, we are able to extrapolate the possible bias on the results of the fits induced by the background. We do not observe any evidence of a bias on the result from this source, when we allow the extra background sample to vary from 1 to 2 percent. A systematic error $\Delta a_2 = 0.004$ is deduced from the fluctuation of the best fit result.

Our measurement of $a_2(\chi_{c1})$ agrees with the value $(a_2 = -0.002\pm_{0.020}^{0.008})$ measured by the Crystal Ball collaboration [9].

B. Results for the χ_{c2}

The full χ_{c2} angular distribution is given in the Appendix (see Table V). The angular distribution, if $a_2, a_3 = 0$ and $B_0^2 = 0$, is given by:

$$W(\cos\theta, \cos\theta', \phi') = \tfrac{1}{10}(1 + \cos^2\theta + \cos^4\theta + 2\cos^2\theta\cos^2\theta' - 3\cos^4\theta\cos^2\theta'$$
$$- \cos^2\theta\sin^2\theta\sin^2\theta'\cos 2\phi' + (\tfrac{1}{4}\sin 2\theta - \sin 2\theta\cos^2\theta)\sin 2\theta'\cos\phi')$$

The data for the χ_{c2} are shown in Fig. 6 and Fig. 7. As for the χ_{c1}, Fig. 6 shows the data compared to the predictions of the fit in the 120 bins of $\cos\theta$, $\cos\theta'$ and ϕ'. Fig. 7 gives the projections of the data on $\cos\theta$, $\cos\theta'$ and ϕ'. The histogram, data points and line have the same meaning as in Fig. 4 above. As an illustration, if $a_2 = 0$ and $B_0^2 = 0$, the projections of the angular distributions reduce to:

$$\bar{W}(\cos\theta) \sim 1 - \frac{1}{3}\cos^2\theta \quad ; \quad \bar{W}(\cos\theta') \sim 1 + \frac{1}{13}\cos^2\theta' \quad ; \quad \bar{W}(\phi') \sim 1 - \frac{8}{71}\cos 2\phi'$$

We fit the data for two different hypothesis for the octupole amplitude a_3. In the first fit, all three parameters are allowed to vary. The octupole amplitude a_3 is found to be consistent with 0. The likelihood function is smooth and well behaved over the whole parameter space. Since the expected value for a_3 is less than 10^{-2}, in the second fit a_3 is set equal to 0 ± 0.005, yielding a systematic error of 0.005 on B_0^2 and of 0.003 on a_2. In both cases, the results of minimum χ^2 and maximum likelihood fits differ by less than 0.25 standard deviations.

After performing the fits, we correct for the bias due to the underlying background. By adding varying numbers of events taken in the h_c (10.9 pb^{-1}) and η_c' (7.2 pb^{-1}) search regions, we estimate the bias on the result due to the background to be:

$$\Delta B_0^2 = -0.03 \pm 0.01, \ \Delta a_2 = -0.009 \pm 0.003, \quad (a_3 \quad \text{fixed} \quad \text{at} \quad 0)$$
$$\Delta B_0^2 = -0.02 \pm 0.01, \ \Delta a_2 = -0.006 \pm 0.004, \ \Delta a_3 = 0.008 \pm 0.004$$

Our best fit results for the $a_3 = 0$ case are $B_0^2 = 0.13 \pm 0.08 \pm 0.013$ and $a_2 = -0.093^{+0.039}_{-0.041} \pm 0.006$. The contour plots of the likelihood function in the a_2-B_0^2 plane for $a_3 = 0$ are shown in Fig. 8. The open point shows the uncorrected best fit value, the solid one shows the final result. The error bars show the systematic error on the final result.

VII. CONCLUSIONS

E835 has studied the formation and radiative decay of χ_{c1} and χ_{c2} states in $\bar{p}p$ annihilation. For the decay process, E835 is the first experiment to give a precise measurement of

the fractional M2 transition amplitude for both J=1 and 2 charmonium P states.

We observe that the value of $a_2(\chi_{c2})$ that we measure is compatible with the predictions of a simple theoretical model. Our value for the χ_{c1} amplitude, however, is lower than expected in this model. Comparing the fractional M2 amplitudes at the χ_{c1} and χ_{c2} gives (assuming $a_3 \equiv 0$):

$$\left.\frac{a_2(\chi_{c1})}{a_2(\chi_{c2})}\right|_{E835} = -0.02 \pm 0.34 \tag{5}$$

which corresponds to a 2 σ discrepancy with respect to equation 2. Figure 9 shows a comparison of all existing measurements of the a_2 amplitude; $\bar{p}p$ experiments indicate a smaller M2 contribution to the χ_{c2} radiative decay, compared to the Crystal Ball result. The observed 2 σ discrepancy could indicate the presence of competing mechanisms, leading to the reduction of the M2 amplitude at the χ_{c1}.

The measurement of $B_0^2(\chi_{c2})$ completes the set of experimental parameters characterizing the coupling of charmonium triplet P states to $\bar{p}p$. Theoretical predictions on the helicity structure of the coupling can be found in the framework of the diquark model [20]. We summarize our information on the helicity dependence of the coupling of $\bar{p}p$ to charmonium in Table III. We characterize the strength of the coupling by the hadronic branching ratio, $BR_h = \Gamma(\chi_{cJ} \to \bar{p}p)/\Gamma(\chi_{cJ} \to \text{hadrons})$. Our present measurement shows that the helicity 0 coupling in the χ_{c2} is small (13%) compared to the helicity 1 contribution. This may be considered consistent with the fact that the χ_{c2} and χ_{c1} coupling to $\bar{p}p$ are quite similar. We note however that the χ_{c0} which couples only through the helicity 0 channel has as large a $\bar{p}p$ coupling as the other states.

VIII.   ACKNOWLEDGMENTS

FULL EXPRESSION FOR THE ANGULAR DISTRIBUTION

The angular distribution for the reactions (1) can be written as

$$W(\theta, \theta', \phi') = \sum_{i=1}^{N} K_i(B_{|\lambda(\bar{p})-\lambda(p)|}, A_{|\lambda(\psi)-\lambda(\gamma)|})T_i(\theta, \theta', \phi') \tag{6}$$

with N=5 at the χ_{c1}, and N=11 at the χ_{c2}. Tables IV(for the χ_{c1}) and V(for the χ_{c2}) give the full expressions (from ref. [10]) for the coefficients K_i and the functions T_i that appear in Eq. 6. The parameter R is defined as:

$$R \equiv \frac{2B_1^2}{B_0^2 + 2B_1^2} = 2B_1^2 = 1 - B_0^2$$

The helicity amplitudes A_k are linear combinations of the multipole amplitudes a_i :

$$\begin{pmatrix} A_0 = \frac{1}{\sqrt{2}}a_1 - \frac{1}{\sqrt{2}}a_2 \\ A_1 = \frac{1}{\sqrt{2}}a_1 + \frac{1}{\sqrt{2}}a_2 \end{pmatrix}_{J=1} \tag{7}$$

$$\begin{pmatrix} A_0 = \sqrt{\frac{1}{10}}a_1 + \sqrt{\frac{1}{2}}a_2 + \sqrt{\frac{6}{15}}a_3 \\ A_1 = \sqrt{\frac{3}{10}}a_1 + \sqrt{\frac{1}{6}}a_2 - \sqrt{\frac{8}{15}}a_3 \\ A_2 = \sqrt{\frac{6}{10}}a_1 - \sqrt{\frac{1}{3}}a_2 + \sqrt{\frac{1}{15}}a_3 \end{pmatrix}_{J=2} \tag{8}$$

REFERENCES

[1] M. Ambrogiani et al. (E835), Phys. Rev. **D60**, 032002 (1999).

[2] T. A. Armstrong et al. (E760), Nucl. Phys. **B373**, 35 (1992).

[3] R. McClary and N. Byers, Phys. Rev. **D28**, 1692 (1983).

[4] G. Karl, S. Meshkov, and J. L. Rosner, Phys. Rev. Lett. **45**, 215 (1980).

[5] M. G. Olsson, C. J. Suchyta, A. D. Martin, and W. J. Stirling, Phys. Rev. **D31**, 1759 (1985).

[6] K. J. Sebastian, H. Grotch, and F. L. Ridener, Phys. Rev. **D45**, 3163 (1992).

[7] H. Grotch, D. A. Owen, and K. J. Sebastian, Phys. Rev. **D30**, 1924 (1984).

[8] T. A. Armstrong et al. (E760), Phys. Rev. **D48**, 3037 (1993).

[9] M. Oreglia et al., Phys. Rev. **D25**, 2259 (1982).

[10] F. L. Ridener, K. J. Sebastian, and H. Grotch, Phys. Rev. **D45**, 3173 (1992).

[11] M. G. Olsson and C. J. Suchyta, Phys. Rev. **D34**, 2043 (1986).

[12] D. Allspach et al., Nucl. Inst. & Meth. **A 410**, 195 (1998).

[13] S. Bagnasco et al., Nucl. Inst. & Meth. **A 409**, 75 (1998).

[14] M. Ambrogiani et al., Nucl. Instrum. Meth. **A419**, 632 (1998).

[15] S. Bagnasco et al., Nucl. Instrum. Meth. **A424**, 304 (1999).

[16] L. Bartoszek et al., Nucl. Inst. & Meth. **A 301**, 47 (1991).

[17] S. Trokenheim et al., Nucl. Instrum. Meth. **A355**, 308 (1995).

[18] W. Baldini et al., Nucl. Instrum. Meth. **A449**, 331 (2000).

[19] D. E. Groom et al. (Particle Data Group), Eur. Phys. J. **C15**, 1 (2000).

[20] M. Anselmino, F. Caruso, and S. Forte, Phys. Rev. **D44**, 1438 (1991).

[21] M. Ambrogiani et al., in preparation (2001).

a_2	χ^2/N_{dof}
0.002±0.032±0.004	87.3/96

TABLE I: Results at the χ_{c1}: the first error is statistical, the second is systematic.

B_0^2	a_2	a_3	χ^2/N_{dof}
$0.16^{+0.09}_{-0.10}$±0.01	$-0.076^{+0.054}_{-0.050}$±0.009	$0.020^{+0.055}_{-0.044}$±0.009	98.9/93
0.13±0.08±0.01	$-0.093^{+0.039}_{-0.041}$±0.006	$\equiv 0$	99.4/94

TABLE II: Results at the χ_{c2}: the first error is statistical, the second is systematic.

State	Helicity 0	Helicity 1	$BR_h * 10^4$
χ_{c2}	0.13±0.08	0.87±0.08	1.2± 0.2 [2]
χ_{c1}	0	1	1.2± 0.2 [2]
χ_{c0}	1	0	1.5-5 [21]

TABLE III: Couplings between $c\bar{c}$ P-states and $\bar{p}p$

i	$T_i(\theta, \theta', \phi')$	$K_i(A_0, A_1)$
1	1	$\frac{1}{2}$
2	$\cos^2\theta$	$\frac{1}{2}(A_1^2 - A_0^2)$
3	$\cos^2\theta'$	$\frac{1}{2}(A_0^2 - A_1^2)$
4	$\cos^2\theta'\cos^2\theta$	$-\frac{1}{2}$
5	$\sin 2\theta \sin 2\theta' \cos\phi'$	$-\frac{1}{4}A_0 A_1$

TABLE IV: Coefficients K_i and functions T_i at the χ_{c1}

$i\ T_i(\theta,\theta',\phi')$	$K_i(R,A_0,A_1,A_2)$
1 1	$\frac{1}{8}(2A_0^2 + 3A_2^2 - R(2A_0^2 - 4A_1^2 + A_2^2))$
2 $\cos^2\theta$	$\frac{3}{4}(-2A_0^2 + 4A_1^2 - A_2^2 + R(4A_0^2 - 6A_1^2 + A_2^2))$
3 $\cos^4\theta$	$\frac{1}{8}(6A_0^2 - 8A_1^2 + A_2^2)(3 - 5R)$
4 $\cos^2\theta'$	$\frac{1}{8}(2A_0^2 + 3A_2^2 - R(2A_0^2 + 4A_1^2 + A_2^2))$
5 $\cos^2\theta'\cos^2\theta$	$\frac{3}{4}(-2A_0^2 - 4A_1^2 - A_2^2 + R(4A_0^2 + 6A_1^2 + A_2^2))$
6 $\cos^2\theta'\cos^4\theta$	$\frac{1}{8}(6A_0^2 + 8A_1^2 + A_2^2)(3 - 5R)$
7 $\sin^2\theta'\cos 2\phi'$	$\frac{\sqrt{6}}{4}(R - 1)A_0 A_2$
8 $\cos^2\theta\sin^2\theta'\cos 2\phi'$	$\frac{\sqrt{6}}{4}(4 - 6R)A_0 A_2$
9 $\cos^4\theta\sin^2\theta'\cos 2\phi'$	$\frac{\sqrt{6}}{4}(5R - 3)A_0 A_2$
10 $\sin 2\theta\sin 2\theta'\cos\phi'$	$-\frac{\sqrt{3}}{4}(A_0 A_1 + \sqrt{\frac{3}{2}}A_1 A_2 - R(2A_0 A_1 + \sqrt{\frac{3}{2}}A_1 A_2))$
11 $\cos^2\theta\sin 2\theta\sin 2\theta'\cos\phi'$	$-\frac{1}{4\sqrt{3}}(5R - 3)(3A_0 A_1 + \sqrt{\frac{3}{2}}A_1 A_2)$

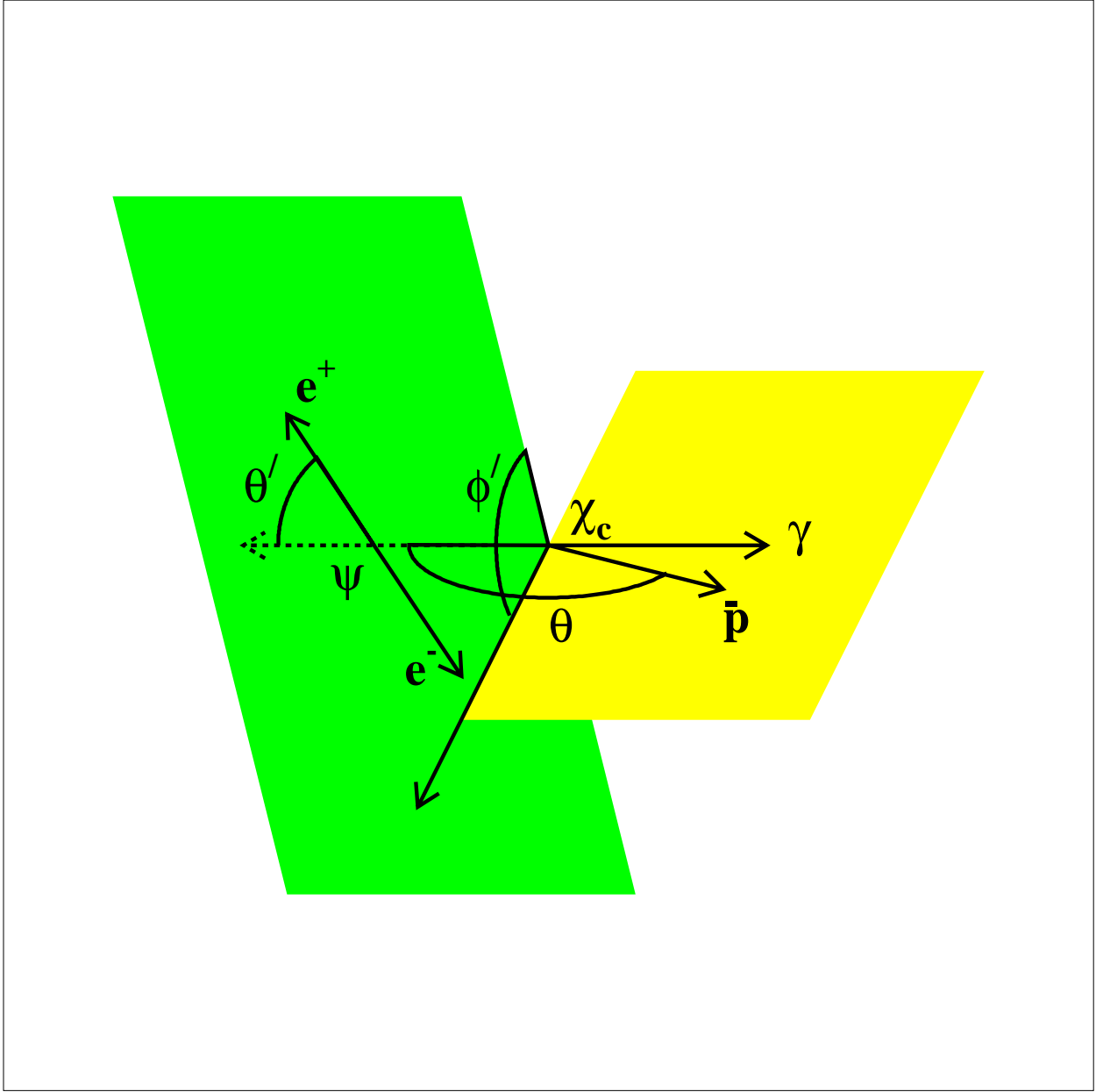TABLE V: Coefficients K_i and functions T_i at the χ_{c2}

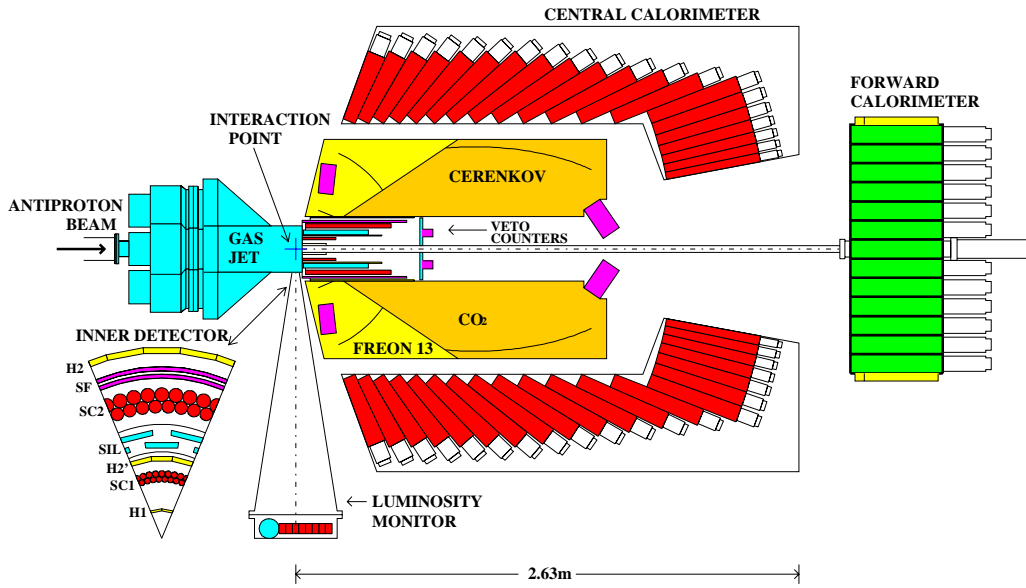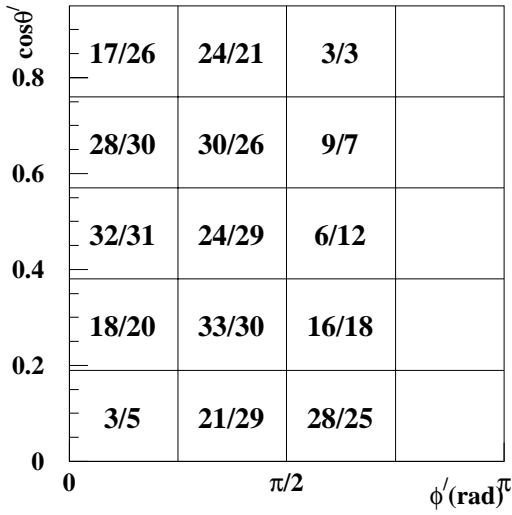FIG. 1: Definition of the angles: θ in the χ rest frame, and θ', ϕ' in the J/ψ rest frame.
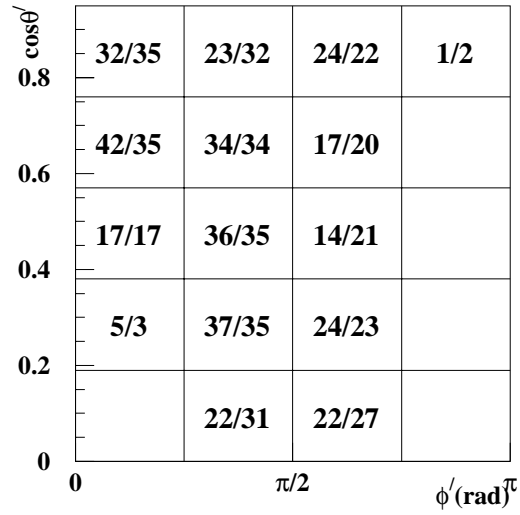
FIG. 2: E835 equipment layout.

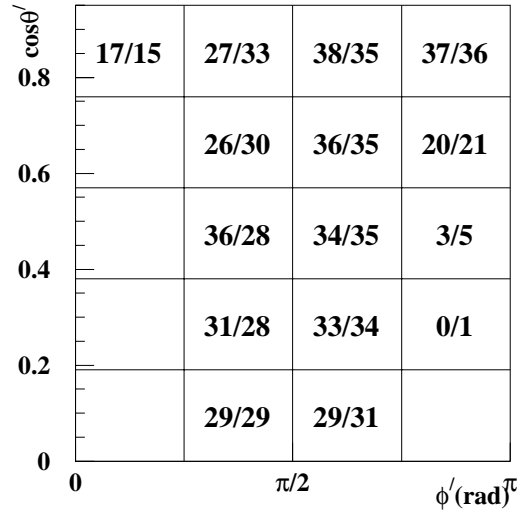# χ_{c1} angular distribution

cosθ=(-0.81,-0.54)

17/26	24/21	3/3
28/30	30/26	9/7
32/31	24/29	6/12
18/20	33/30	16/18
3/5	21/29	28/25

cosθ=(-0.54,-0.27)

32/35	23/32	24/22	1/2
42/35	34/34	17/20	
17/17	36/35	14/21	
5/3	37/35	24/23	
	22/31	22/27	

cosθ=(-0.27,0)

40/34	34/35	30/33	27/21
17/13	34/35	47/32	3/3
3/1	29/34	28/30	
	29/31	32/28	
	37/29	31/28	

cosθ=(0,0.27)

17/15	27/33	38/35	37/36
	26/30	36/35	20/21
	36/28	34/35	3/5
	31/28	33/34	0/1
	29/29	29/31	

cosθ=(0.27,0.54)

19/21	29/32	26/35
27/20	35/34	40/37
25/23	49/35	17/25
26/26	36/36	5/8
33/30	26/34	1/1

cosθ=(0.54,0.81)

2/4	17/15	14/17
13/7	16/17	19/20
14/10	15/19	21/21
19/14	25/19	18/15
22/18	16/19	3/4

Axis labels: $\cos\theta$ (vertical), $\phi'(\mathrm{rad})$ (horizontal), with markings at 0 and $\pi/2$.
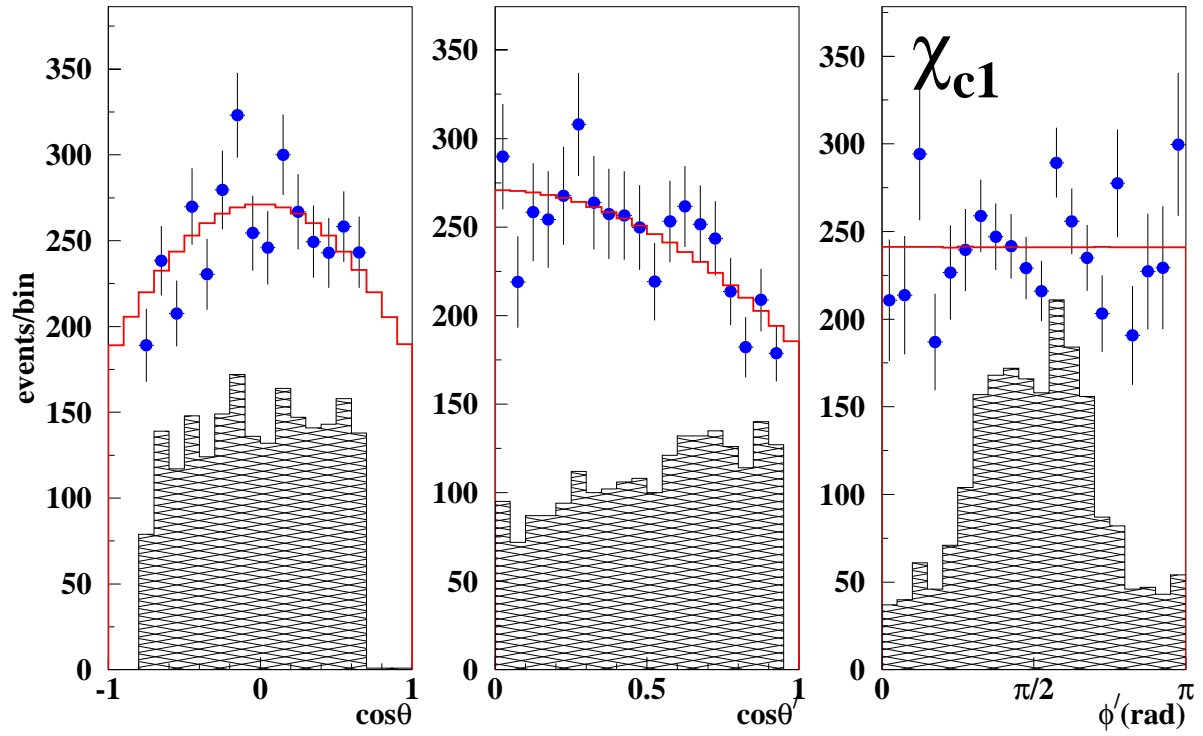
FIG. 4: Projections of the angular distribution at the χ_{c1}: the data sample, corrected for acceptance (dots), is compared to the best fit prediction (solid line). The raw data set (shaded histogram) is also shown.
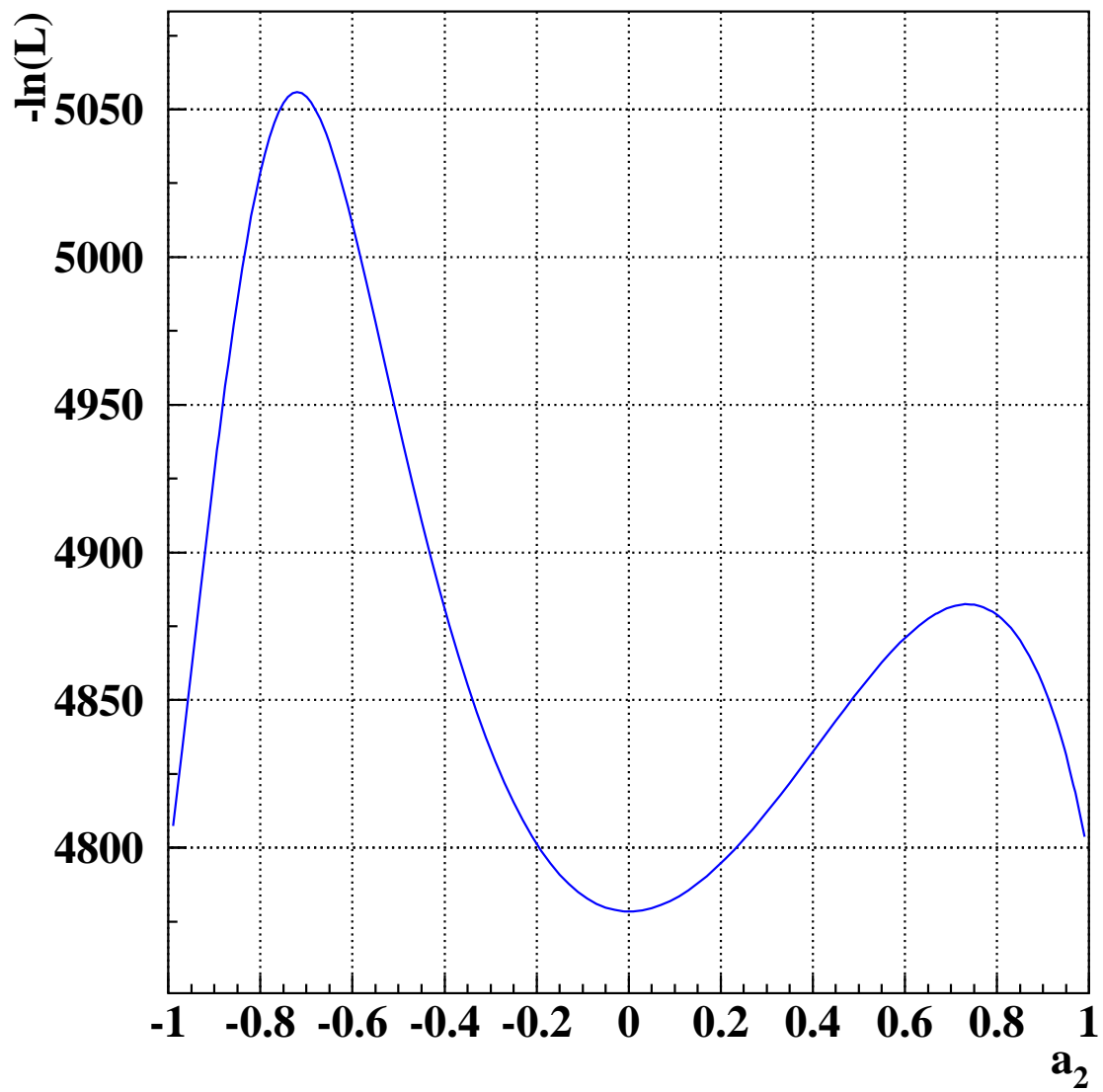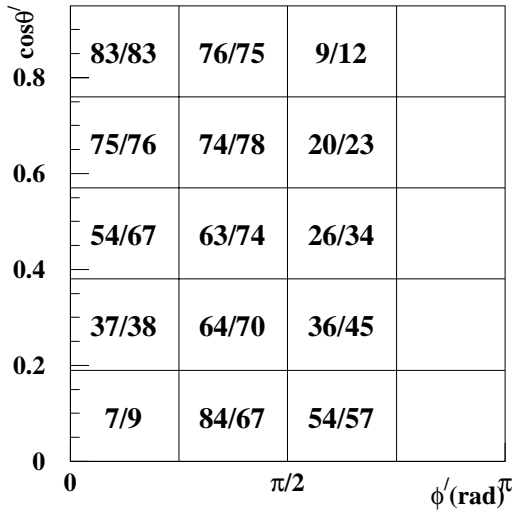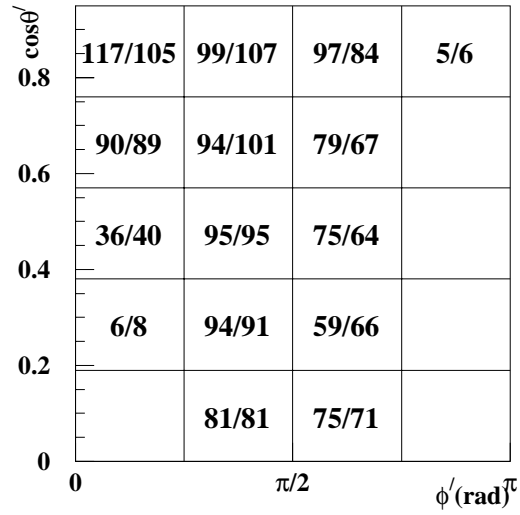
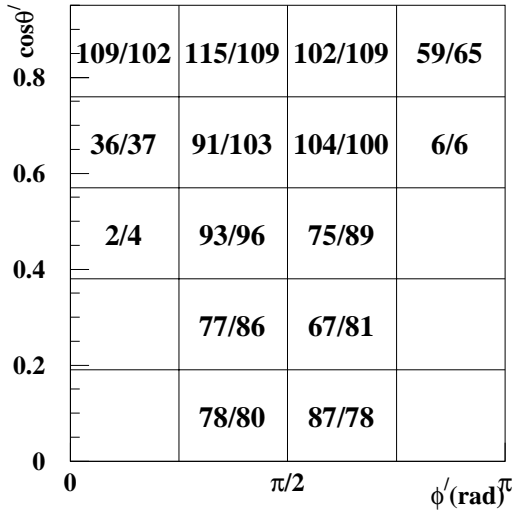FIG. 5: For the χ_{c1}, $-\ln\mathcal{L}(a_2)$ as function of a_2

χ_c2 angular distribution

cosθ=(-0.81,-0.54)

cosθ \ φ'(rad)			
0.8	83/83	76/75	9/12
0.6	75/76	74/78	20/23
0.4	54/67	63/74	26/34
0.2	37/38	64/70	36/45
	7/9	84/67	54/57

cosθ=(-0.54,-0.27)

cosθ \ φ'(rad)			
0.8	117/105	99/107	97/84	5/6
0.6	90/89	94/101	79/67	
0.4	36/40	95/95	75/64	
0.2	6/8	94/91	59/66	
		81/81	75/71	

cosθ=(-0.27,0)

cosθ \ φ'(rad)			
0.8	109/102	115/109	102/109	59/65
0.6	36/37	91/103	104/100	6/6
0.4	2/4	93/96	75/89	
0.2		77/86	67/81	
		78/80	87/78	

cosθ=(0,0.27)

cosθ \ φ'(rad)			
0.8	70/51	102/109	94/109	86/105
0.6	2/2	99/95	97/103	56/51
0.4		80/83	100/98	11/10
0.2		82/79	81/92	1/1
		84/81	87/85	

cosθ=(0.27,0.54)

cosθ \ φ'(rad)			
0.8	3/2	81/77	117/107	123/105
0.6		66/67	86/100	95/92
0.4		55/69	92/95	67/52
0.2		69/72	96/91	23/15
		68/78	91/86	0/1

cosθ=(0.54,0.81)

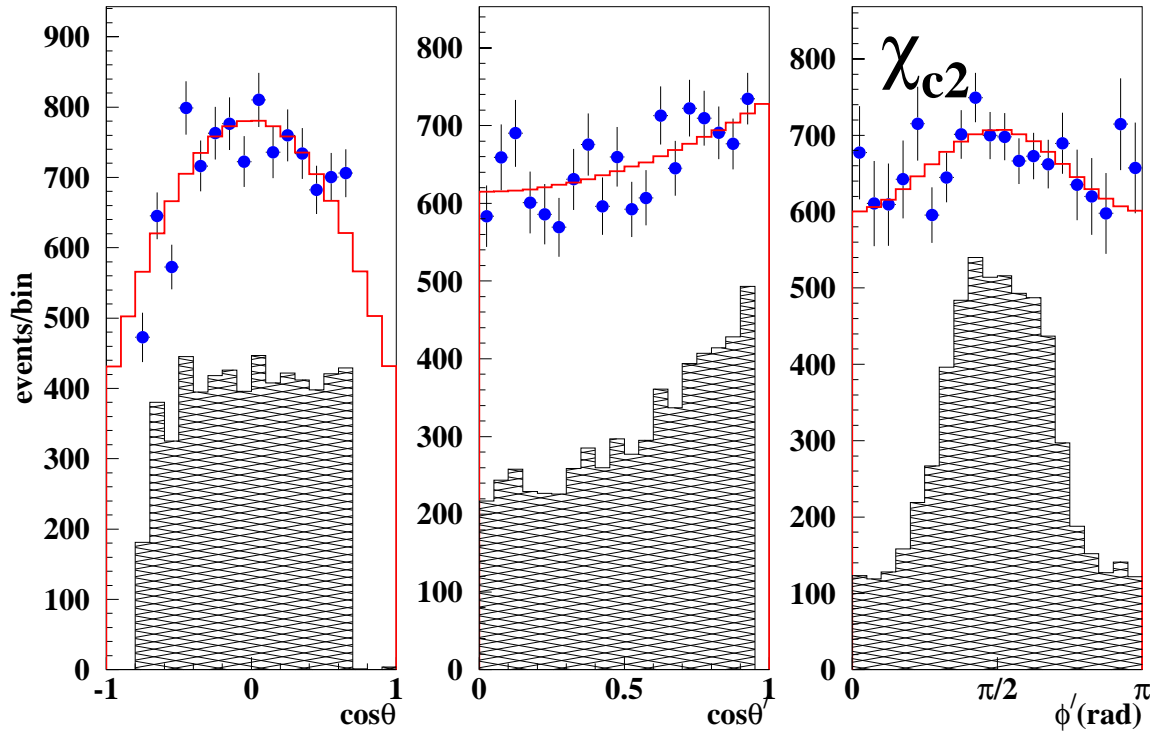| cosθ \ φ'(rad)			
0.8		16/16	48/58	57/59
0.6		23/25	73/56	63/54
0.4		36/30	65/53	51/48
0.2		36/36	63/50	30/29
		55/44	45/48	13/8

22

FIG. 7: Projections of the angular distribution at the χ_{c2}: the data sample, corrected for acceptance (dots), is compared to the best fit prediction (solid line). The raw data set (shaded histogram) is also shown.
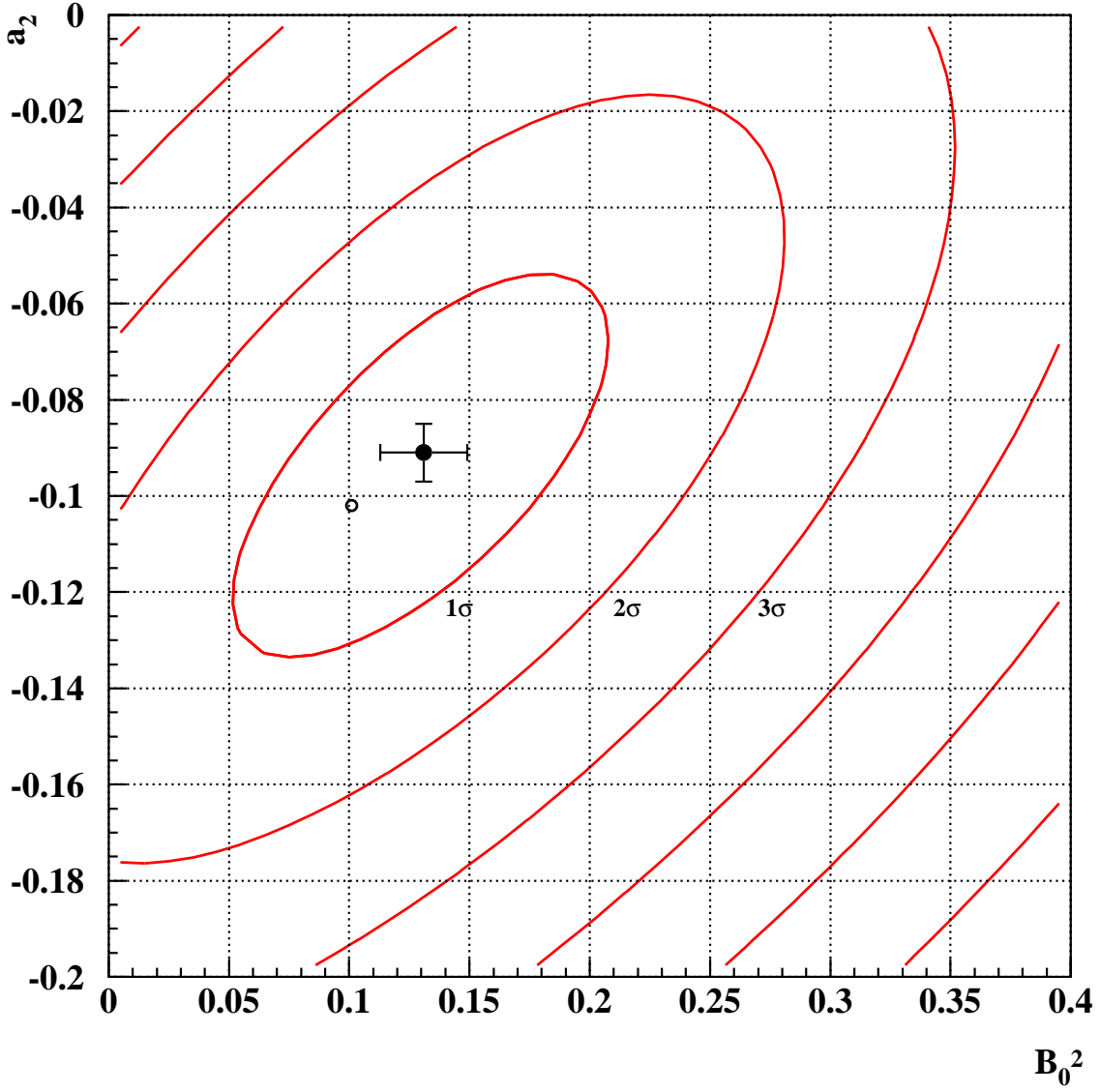
FIG. 8: Contour lines of $\ln\mathcal{L}(a_2, B_0^2)$, corresponding to 1,2,3... standard deviations around the best fit value for the χ_{c2}, when a_3 is set equal to 0. The open marker indicate the best fit result before correcting for the bias. The error bars show the size of the total systematic error.
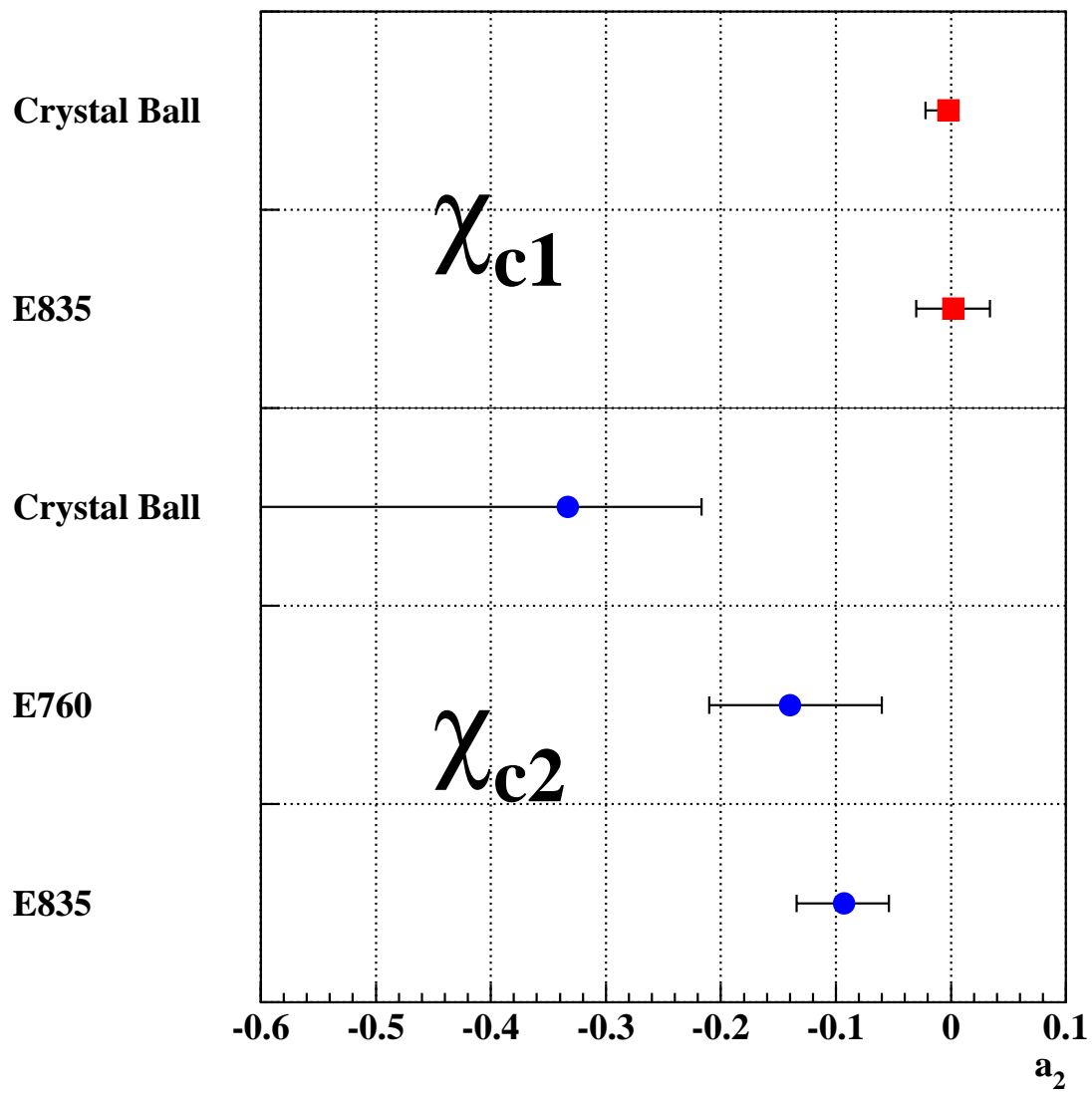
FIG. 9: Results from Crystal Ball [8], E760 [7] and E835 for $a_2(\chi_{c1}, \chi_{c2})$